Mirages with atmospheric gravity waves

Waldemar H. Lehn, Wayne K. Silvester, and David M. Fraser

The temperature inversions that produce superior mirages are capable of supporting gravity (buoyancy) waves of very low frequency and long wavelength. This paper describes the optics of single mode gravity waves that propagate in a four-layer atmosphere. Images calculated by ray tracing show that (1) relatively short waves add a fine structure to the basic static mirage, and (2) long waves produce cyclic images, similar to those observed in the field, that display significant variation from a base image.

Key words: Mirages, atmospheric gravity waves.

1. Introduction

Mirages observed over an interval of time occasionally display slow variations that seem to be periodic. This can be seen in Fig. 1, a sequence photographed at Tuktoyaktuk, Northwest Territories, Canada, on 16 May 1979. The images show mirages of Whitefish Summit, a low hill at a distance of 20 km, whose normal appearance is shown in Fig. 2. The mirages move through a sequence of shapes that roughly repeats itself.

The time at which each photograph was made is shown on the images; the time zone is Mountain Daylight Time. At the time we did not suspect any periodicity, hence the times are not at uniform intervals. That is also why the sequence ends abruptly (at 3:30 a.m.). Considering the similarity between Figs. 1a and 1g, one could say that this interval of ~28 min is one period. Although the second cycle does not duplicate the first, there are significant points of similarity between the corresponding images of Figs. 1c and 1i in the top and the bottom thirds of the mirage.

Another point of importance is the appearance of repetitive fine structures in Figs. 1b and 1h, which show up as jagged edges in Figs. 1f and 1i.

As the observer and the target object are both stationary, the changing images imply some kind of periodic motion in the atmosphere. A candidate for this motion is the atmospheric gravity wave[1] (buoyancy wave), which can exist in stratified atmospheres of the type that produces mirages. The frequencies of gravity waves can be low enough to fit the observed time scale (minutes to tens of minutes). Fraser[2] uses them to explain sun images with jagged edges. However, to our knowledge, no previous work has been done to calculate and study such images. The purpose of this paper is to investigate the nature of image modifications produced by gravity waves and to compare the computations with field observations.

2. Gravity Waves

Gossard and Hooke[3] derive the equations of motion for gravity waves that are used here. This section follows their development and notation.

Initially the atmosphere is considered stably stratified and spherically symmetric, concentric with the earth. The temperature profile is an inversion, which is necessary for the superior mirage. Variations in pressure, velocity, and temperature are considered slow, as well as small, relative to their equilibrium values. This permits the use of linearized equations. If we further consider any waves to be propagating in the x–z plane (by choice of coordinates: x along the line of sight, z vertical) then the problem becomes two dimensional. The differential equations for the motion are

$$\frac{\partial u}{\partial t} = -\frac{1}{\rho_0}\frac{\partial p}{\partial x}, \tag{1}$$

$$\frac{\partial w}{\partial t} = -\frac{1}{\rho_0}\frac{\partial p}{\partial z} - g\frac{\rho}{\rho_0}, \tag{2}$$

$$\frac{\partial \rho}{\partial t} + w\frac{\partial \rho_0}{\partial z} = 0, \qquad \frac{\partial u}{\partial x} + \frac{\partial w}{\partial z} = 0, \tag{3}$$

The authors are with the Department of Electrical and Computer Engineering, University of Manitoba, Winnipeg, Manitoba R3T 5V6, Canada.

Received 1 October 1993; revised manuscript received 19 January 1994.

0003-6935/94/214639-05$06.00/0.

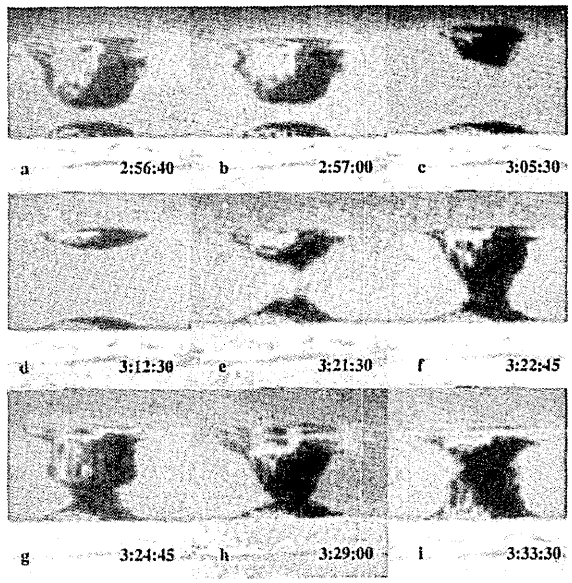

Fig. 1. Mirages of Whitefish Summit, seen from Tuktoyaktuk, Northwest Territories, Canada, on 16 May 1979. The numbers indicate Mountain Daylight Time.

where u, w are the x and z velocity perturbations from equilibrium, ρ and p are density and pressure perturbations, respectively, ρ_0 is the reference (equilibrium) density, and g is the acceleration of gravity.

The equations of motion are satisfied by wave solutions for u, w, and p. In particular, $w = w_z \exp[i(kx - \omega t)]$ and $p = p_z \exp[i(kx - \omega t)]$, where w_z and p_z (functions of z only) have the form $\exp(\frac{1}{2}\alpha z)[A \exp(i\eta z) + B \exp(-i\eta z)]$. The spatial frequency η is related to the Vaisala–Brunt frequency N by

$$\eta^2 = \frac{k^2}{\omega^2}(N^2 - \omega^2) - \Gamma^2, \tag{4}$$

where N itself depends on the temperature gradient:

$$N^2 = \frac{g}{T}\left(\frac{g}{c_p} + \frac{dT}{dz}\right). \tag{5}$$

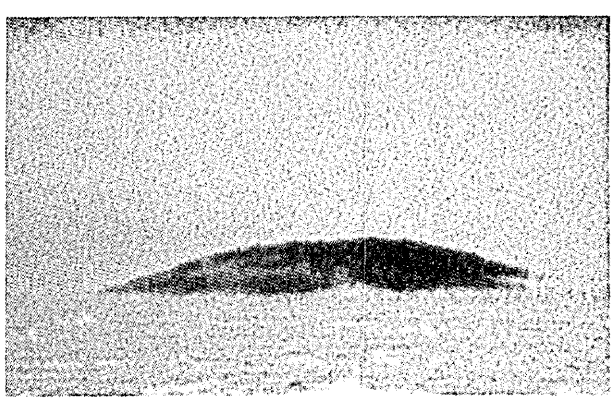

Fig. 2. Normal appearance of Whitefish Summit over the same line of sight as in Fig. 1.

The function Γ is given by

$$\Gamma = -N^2/2g + g/2c_s^2. \tag{6}$$

The parameter α, which is given by

$$\alpha = -\frac{1}{\rho_0}\frac{\partial \rho_0}{\partial z}, \tag{7}$$

is assumed to be constant, i.e., the reference density ρ_0 is an exponential function of z, with scale height $1/\alpha$. As the atmosphere's scale height is ~ 8000 m, α is very small, and the exponential is nearly equal to unity for z below 100 m. Further, c_s is the speed of sound, and c_p is the specific heat of air at constant pressure.

The model used here consists of four layers of constant temperature gradient with no wind shear; it is based on a three-layer case study by Gossard and Hooke.[4] Four layers are sufficient to approximate actual inversions quite well. Figure 3 shows the four-layer approximation to a temperature profile that was calculated to reproduce the mirage of Fig. 1e under static conditions.[5] The dispersion equation that relates k and ω (i.e., that identifies waves that the system can support) is then found by the requirement that all four layers have the same x,t dependence (the complex exponential given above) and by application of conditions of continuity on w_z and $\partial w_z/\partial z$ at the internal layer boundaries. At the ground ($z = 0$) and at the atmosphere's upper limit, w_z is zero. The first few solutions (the lowest-order modes) for the four-layer model of Fig. 3 are shown in Fig. 4. Although natural waves can consist of linear combinations of several modes, this study considers only single mode waves. Selection of a specific k, ω pair permits the four amplitude functions w_z to be found for the layers to within a common multiplicative constant. These

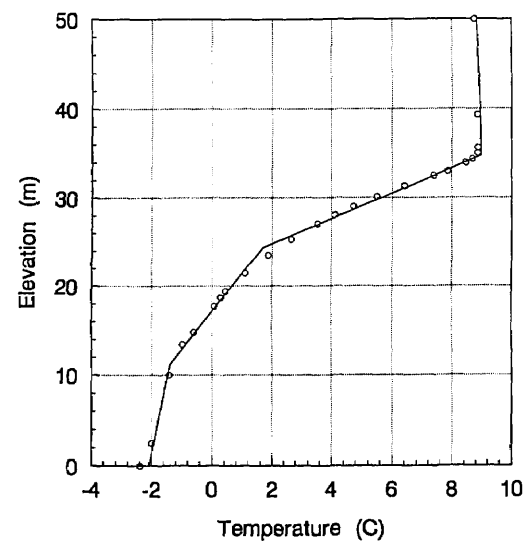

Fig. 3. Four-layer piecewise linear profile (solid curve) fitted to a temperature profile (open circles) that produces the mirage of Fig. 1e.

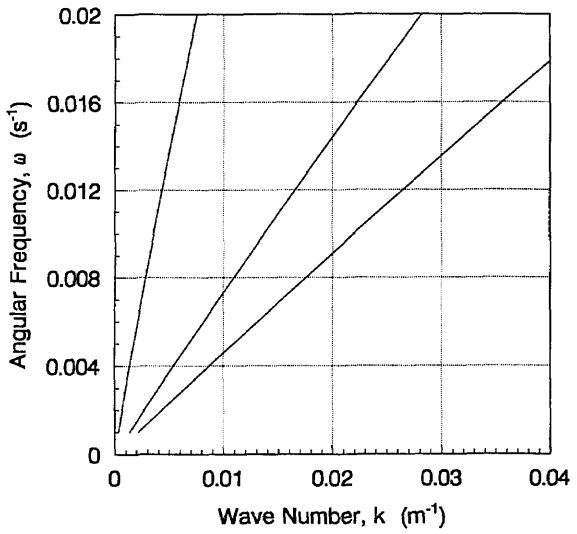

Fig. 4. Solutions to the dispersion equation for the four-layer model of Fig. 3; the three lowest-order modes are shown.

solutions give the incremental vertical velocity components at each elevation; integration of w with respect to t gives the vertical displacement from equilibrium.

The motion is considered to be adiabatic. The isotherms of the undisturbed atmosphere, originally at constant elevations above the Earth's surface, now take on the sinusoidal shapes given by the wave solutions. The wave amplitude derived from the four-layer model is applied to each corresponding point of the actual profile. A typical wave plot is shown below with the examples (Fig. 6).

3. Ray Tracing

We calculate mirage images by tracing a bundle of light rays projected from the observer's eye. The atmosphere is modeled as a set of concentric spherical shells. The temperature profile, required by the program as input data, specifies a set of elevations and their temperatures. These elevations define isotherms that form the boundaries between the spherical shells (layers). The temperature is continuous and varies linearly within the layer; with a sufficient number of points the piecewise linear profile approximates a smooth natural profile quite well.[6]

To calculate the waves, we fit a four-layer model to the input temperature profile, as we did in Fig. 3. An off-line Mathcad program is used to find η for each layer and to solve the dispersion equation (input ω, find k). Then the wave amplitudes are found, and the appropriate four-layer solution is applied to each elevation in the input profile. For the values used in the calculations, wave amplitudes of a few meters and wavelength of a few kilometers, the layer slopes are sufficiently small that the normal to each layer can be taken as vertical. Temperature between the (now sinusoidal) isotherms is linearly interpolated in the vertical direction. As pressure changes very little over the wave amplitude, pressure values at the static layer levels are used.

The general form[7] for local ray curvature κ is

$$\kappa = \frac{1}{n}\hat{\nu}\nabla n, \tag{8}$$

where n is the refractive index of air, and $\hat{\nu}$ is the unit normal to the ray path. It becomes

$$\kappa = \frac{\epsilon\rho}{nT}\left(g\beta + \frac{dT}{dz}\right)\cos\phi \tag{9}$$

when gradients are approximated as vertical. Here, ϕ is the ray slope angle, and ϵ and β are constants (226×10^{-6} and 3.48×10^{-3}, respectively). To simplify the computation, we approximate the rays as sequences of short parabolic arcs; the Earth's surface is similarly represented. Every time a ray intersects an isotherm, parameters are recalculated, and a new arc is begun. The intersection of the ray bundle with the target determines the nature of the image seen by the observer, as the eye interprets the rays as straight.

4. Nature of the Images

The photographic subject of the two cases below is Whitefish Summit. It is one of many low, rounded hills, locally known as pingos, that rest upon remnants of glacial ice. The map of Fig. 5 shows the locations of Tuktoyaktuk and Whitefish Summit on the shores of the Beaufort Sea. The 20-km line of sight, from an observer elevation of 2.5 m, passes entirely over sea ice. Aside from the pingos, the landscape to the south is relatively flat; in this region there is no elevation above 50 m within 15 km of the coast. Various estimates exist for the peak elevation of Whitefish Summit. For this analysis the value of 18.7 m, which is based on the average of numerous theodolite measurements from Tuktoyaktuk, is used. The exact value is not critical to the conclusions because the atmospheric model can be suitably scaled. At the time of the observations of Fig. 1 (case 2 below) there was no noticeable wind. However, it seems intuitive that a slow drift of air from the south over

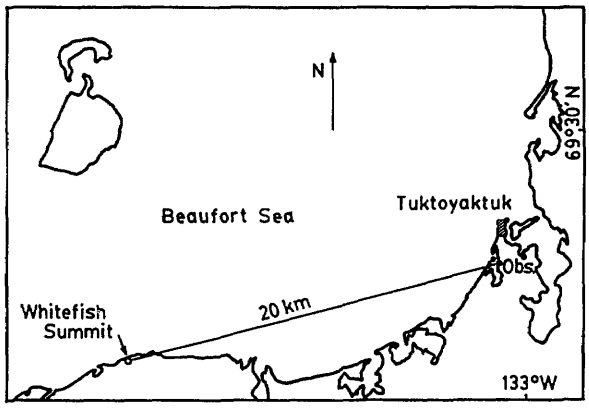

Fig. 5. Map of the Tuktoyaktuk region.

the slightly undulating landscape could be the source of the gravity waves.

A. Case 1

This example demonstrates the jagged-edge effect by artificial application of a gravity wave to a static mirage. As mentioned in Section 2, the static reconstruction of Fig. 1e produced the atmosphere whose temperature profile is shown in Fig. 3. Figure 3 also shows the four-layer approximation used to generate a gravity wave, which is assumed to travel along the line of sight. The wave frequency ω was arbitrarily selected to be 0.004 s^{-1}, for which the corresponding period of 26 min roughly matches the observed period of the Fig. 1 sequence. The corresponding lowest-mode wave number, from Fig. 4, is $k = 0.00139$ m^{-1}; the wavelength is 4530 m. It should be noted that this wavelength is a lower bound for this mode: if the wave vector were not parallel to the line of sight, the apparent wavelength experienced by the light rays would increase. This concept is applied in case 2.

The vertical wave numbers (η values) for the lowest three layers, starting at the bottom, are 0.0174, 0.0324, and 0.0548 m^{-1}, whereas in the top layer the vertical wave decays as $\exp(-0.00171z)$. Wave amplitude at elevation 11.2 m is 2.0 m. To give an impression of the ray paths through the waves, a few rays and waves are shown in Fig. 6 (the observer is at $x = 0$); the actual calculation uses a far larger number of each. The wave has the given position at $t = 0$; it is advanced to the right by quarter wavelengths to produce four different images. Each image is determined by its transfer characteristic (TC), which is a mapping of apparent ray elevation versus actual ray elevation in the target plane. Figure 7 shows the four quarter-period TC's, as well as the one for the static case (no waves). Although it is difficult to isolate the TC for each wave, Fig. 7 shows the trend: all four have the same overall shape, with small differences in fine structure. The waves create these fine irregularities; as the waves advance, the irregularities shift around, but change little in size. Further, the wave TC's are similar to the static TC, except at the top, where the waves permit light rays with large initial angles (refracted downward by the static atmosphere) to escape upward out of the inversion. The four quarter-period images, which were calculated by means of a mirage simulator program,[8] are seen in Fig. 8; they should be compared with the static equivalent, Fig. 1e. It can be seen that the static and the wavy images have rather similar shapes; however, the small ray deflections produced by the waves create the jagged edges.

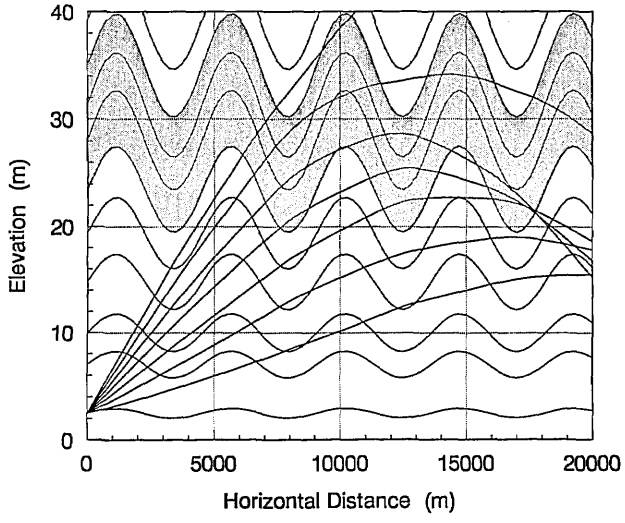

Fig. 6. Selected waves and rays for the example of case 1. The rays receive most of their deflection in the zones of highest temperature gradients, which are shaded (see also Fig. 3). The initial ray elevation angles span the range from 2 to 14 arcmin, in 2′ steps.

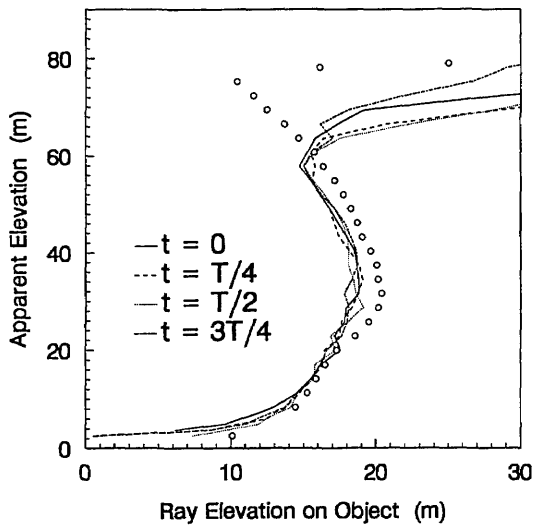

Fig. 7. Comparison of TC's. The open circles show the TC in the absence of waves; the remaining four curves correspond to wave positions at successive quarter-periods.

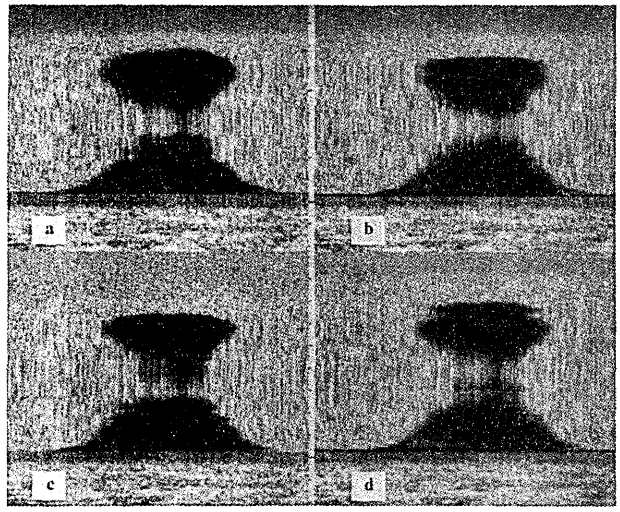

Fig. 8. Mirages calculated by application of the TC's of Fig. 7 to the normal image of Whitefish Summit (Fig. 2).

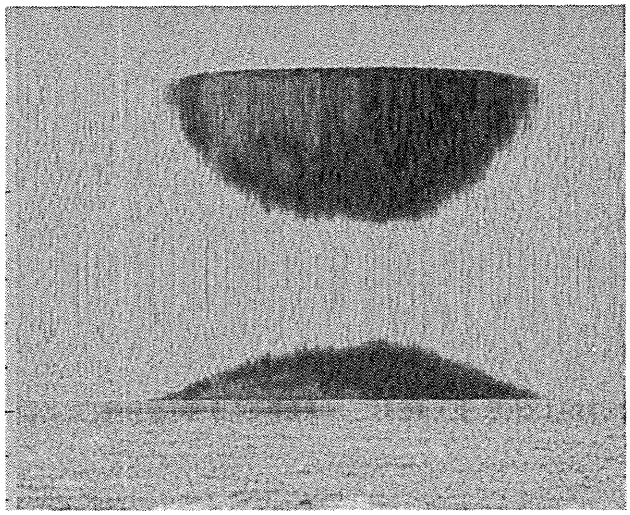

Fig. 9. Reference image (without waves) for case 2.

B. Case 2

In this example, an attempt is made to reconstruct the first period of the whole observed sequence of Fig. 1. This image sequence can be viewed as a set of deviations from a base or average image that would be seen in the static case. We create such an image, shown in Fig. 9, by experimentally manipulating a TC and running the mirage simulator. Next the corresponding temperature profile is obtained, to which the four-layer model is fitted; see Fig. 10. The same frequency as in case 1 is used: $\omega = 0.004\ s^{-1}$. But now a k value lower than that given by the dispersion equation is used: $k = 0.0007\ m^{-1}$ ($\lambda = 9000$ m). To a first approximation this can be justified by considering that the wave is propagating at an angle to the line of sight, rather than along it. Here the wave vector would make an angle of 60° with the sight line. For a wave amplitude of 2.5 m at 14 m, the images at one-eighth wavelength intervals are shown in Fig. 11. A more radical change of shape is observed because the very long waves have a length and a shape rather similar to the upper arcs of the rays and interact strongly with them. The base mirage can be seen to grow and shrink as the wave passes. The calculated sequence bears reasonable resemblance to Fig. 1.

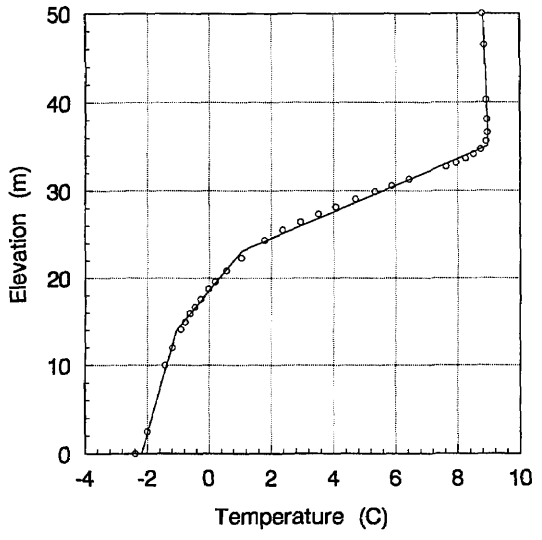

Fig. 10. Four-layer fit (solid curve) to the temperature profile (open circles) that generates the reference image.

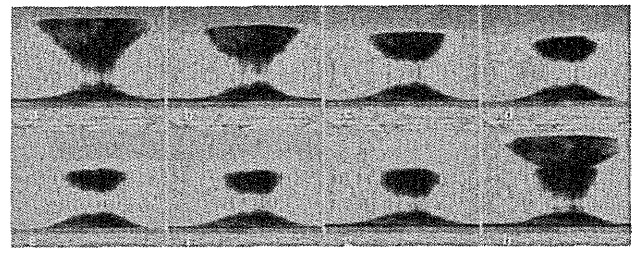

Fig. 11. Mirage sequence that approximates the observed sequence of Fig. 1. The wave advances by one-eighth wavelength between successive images.

5. Conclusion

The gravity wave mirage model produces images very similar to those observed in the field. For waves of relatively short wavelength, for which many cycles exist in the optical path, the waves produce a spatially repetitive fine structure most often seen as jagged edges. For longer wavelengths, with only one or two cycles in the line of sight, significant periodic changes occur in the images, which can be interpreted as deviations from an average image that would be seen in the static case. The calculated shape varies in a manner similar to that observed in nature.

This research was supported in part by the Natural Sciences and Engineering Research Council of Canada.

References

1. J. Lighthill, *Waves in Fluids* (Cambridge U. Press, Cambridge, 1978), Chap. 4, pp. 284–316.
2. A. B. Fraser, "The green flash and clear air turbulence," Atmosphere **13**, 1–10 (1975).
3. E. E. Gossard and W. H. Hooke, *Waves in the Atmosphere* (Elsevier, New York, 1975), Chap. 2, pp. 75–77.
4. Ref. 3, Chap. 5, pp. 150–156.
5. W. H. Lehn, "Inversion of superior mirage data to compute temperature profiles," J. Opt. Soc. Am. **73**, 1622–1625 (1983).
6. W. H. Lehn, "A simple parabolic model for the optics of the atmospheric surface layer," Appl. Math. Model. **9**, 447–453 (1985).
7. O. N. Stavroudis, *The Optics of Rays, Wavefronts, and Caustics* (Academic, New York, 1972), Chap. III, p. 38; curvature is found by taking the dot product of Eq. (III-10) with the unit normal $\hat{\nu}$.
8. W. H. Lehn and W. Friesen, "Simulation of mirages," Appl. Opt. **31**, 1267–1273 (1992).